Local comparison of multimodal medical surfaces using a new variational splines fitting algorithm

Ahmad Almhdie, Christophe Léger

Local Comparison of Multimodal Medical Surfaces using a New Variational Splines Fitting Algorithm

Ahmad Almhdie-Imjabber[1,2], Christophe Léger[1]
[1]*Institut PRISME, Université d'Orléans*
[2]*Electrical and Electronic Department, University of Sebha, Libya*
Ahmad.Almhdie@univ-orleans.fr, Christophe.Leger@univ-orleans.fr

Abstract

In this paper, we propose a modified variational splines fitting (MVSF) algorithm for the reconstruction and comparison of medical surfaces. The MVSF algorithm presents the advantage to use high precise and low complex approximation of the equations of energy in the discrete temporal domain, compared to previously presented methods. It also takes into account the periodicity constraints encountered when reconstructing sphere-like shape closed surfaces. Moreover, it gives straightly the mean square error (MSE) between the original data and the reconstructed data, which is useful to quantify the approximation introduced by the reconstruction. The developed model has been successfully applied for real biomedical data; in particular for the reconstruction and comparison of the left ventricle of human heart, acquired by SPECT and ultrasound imaging modalities.

Keywords: Local comparison, multimodal, surface fitting, surface reconstruction.

1. Introduction

Surface reconstruction is a step generally carried out before comparing or representing/ visualizing discrete data sets. It is essential when the two data sets to be compared present dissimilar numbers of samples, different sampling processes, or missing samples (sparse data). These cases are commonly encountered in medical imagery, and particularly in the comparison of data obtained from several imaging modalities [1]. Hence, it is necessary to carry out resamplings, using interpolation and/or smoothing methods.

Surface reconstruction and smoothing methods are widely used in practice to best estimate the original surface represented by a scattered noisy point. For instance, the number and the distribution of the initial samples of an organ surface lead to incomplete meshes. Stacks of two-dimensional contours can also be used to reconstruct three-dimensional surfaces [2].

The problem of surface reconstruction can be solved using a variety of techniques. The finite element method is one of these techniques. An example of this method is the use of Voronoi diagram and Delaunay triangulation [3] to find the topological connection of the sample points. Fourier-based interpolation methods [4], to mention a few, are also used in the domain of surface reconstruction.

Another type of reconstructing smooth surfaces relies on the finite difference methods using deformable models [5] such as thin plate model [6]. The main idea is to create an initial mesh and deform it to best match the range input data. This is usually expressed as an energy minimization problem. There are two forces that formulize the final shape of the reconstructed surface. One attracts the surface towards the input data and the other tries to keep the surface smooth. These methods are generally computationally inexpensive but comparably more sensitive to number of missing points. The former approach was selected for further study in this work as it is generally more appropriate for smooth surfaces such as surfaces of left ventricle of heart. In general, methods based on deformable models give nice smooth surfaces but are computationally expensive and complex. We present in this work a faster and less complex algorithm compared to a previous algorithm proposed by Richard Szeliski. The reconstruction step makes it easier to compare medical surfaces obtained by different modalities or at different time or position.

The next section concerns the description of the original VSF method and our proposed variant, required prior to local comparison of medical surfaces with incomplete samples. Data used in our experiments are described in section 3. Results are then presented and discussed. Finally, conclusions are given.

2. Variational Splines Fitting (VSF) Algorithm

In [7], the author proposed to use a deformable model (here we call it VSF) to estimate the missing points. In this model, the problem is formulated as an optimization one. The function to be minimized is written.

$$E(x) = E_d(x) + \lambda E_s(x) \qquad (1)$$

Where $X = [X_{i,j}]$, (i = 0 : N-1, j = 0 : M-1) are the mesh regular points of the reconstructed surface, i and j indicate spatial positions. This function includes two constraints: the data compatibility constraint $E_d(X)$, and the smoothness constraint $E_s(X)$. The above formulation is usually expressed as an energy minimisation problem where an attracting force draws the mesh towards the sparse data « $E_d(x)$ » and a tension in the mesh keeps the surface smooth « $E_s(x)$ » [2]. λ ($\lambda>0$) is the regularization parameter which is used to adjust the closeness of the fit between the surface and the sparse data set. Figure 1 shows an example of a 2D curve construction under the effect of the regularisation parameter. This parameter depends on the sparse data set and can be estimated using a generalised cross validation technique. In general, as λ increases, the reconstructed surface becomes smoother. However, the probability of error between the original sparse samples and their corresponding estimated ones becomes higher. For very high values of λ, ($\lambda \to \infty$), the fitted surface tends towards a flat one. As λ tends to zero, this probability becomes smaller, but the reconstructed surfaces might no longer be smooth.

Figure 1 : Smoothing degree of reconstructed surfaces in function of λ : λ_1 (a) > λ_2 (b).

The data compatibility constraint measures the distance between the original sparse points and the interpolated smooth surface. The energy expression corresponding to the data compatibility constraint can be written as:

$$\varepsilon_d(x) = \frac{1}{2}\sum_i w_i (f(u_i, v_i) - d_i)^2 \qquad (2)$$

The discrete form is:

$$E_d(\mathbf{x}, \mathbf{d}) = \frac{1}{2}\sum_{(i,j)} \mathbf{w}_{i,j} (\mathbf{x}_{i,j} - \mathbf{d}_{i,j})^2 \qquad (3)$$

where $\mathbf{x}_{i,j}$ stands for the discrete values of $f(u_i,v_i)$: $\mathbf{x}_{i,j} = f(u_i,v_i)$, $\mathbf{d}_{i,j}$ ($\mathbf{d}_{i,j}$ = 0 at missing points) are the sparse samples of the original incomplete surface and the weights $w_{i,j}$ ($w_{i,j}$= 0 at missing points) are inversely related to the variance of the measurements. The higher the weights, the better the reconstructed surface fits the original sparse samples. In this case, the data compatibility constraint over influences the overall energy function and the reconstructed surface become no longer smooth.

Reassembling all mesh points into a vector x, one can rewrite equations (3) in a matrix form. The energy corresponding to the data compatibility constraint becomes:

$$E_d(\mathbf{x},\mathbf{d}) = \frac{1}{2}(\mathbf{x}-\mathbf{d})^T \mathbf{A}_d (\mathbf{x}-\mathbf{d}) \qquad (4)$$

where $\mathbf{d}$ is a zero-padded vector of data values and the diagonal matrix $\mathbf{A}_d$ has entries w_i at which the data coincide with the sparse data points and zeros elsewhere. In particular, this allows treating problems with missing or unknown data. Using the thin plate model, the energy function corresponding to the smoothness constraint can be written in continuous form as:

$$\varepsilon_s(f) = \frac{1}{2}\int\int \left(f_{uu}^2 + f_{vv}^2 + 2f_{uv}^2\right) du dv \qquad (5)$$

where *f: f(u,v)* is the smoothed continuous functional of the interpolated surface in u and v directions; and the subscripts uu, vv and uv indicate partial derivatives.

2.1. Original VSF algorithm

In the original VSF algorithm, the discrete form of the above energy function is derived using a classical finite-difference scheme. The resulting discrete function is:

$$E_s(x) = \frac{h_u h_v}{2}\sum_{i,j}\left[\left(\frac{\mathbf{x}_{i+1,j} - 2\mathbf{x}_{i,j} + \mathbf{x}_{i-1,j}}{h_u^2}\right)^2 + \left(\frac{\mathbf{x}_{i,j+1} - 2\mathbf{x}_{i,j} + \mathbf{x}_{i,j-1}}{h_v^2}\right)^2 + 2\left(\frac{\mathbf{x}_{i+1,j+1} - \mathbf{x}_{i,j+1} - \mathbf{x}_{i+1,j} + \mathbf{x}_{i,j}}{h_u h_v}\right)^2\right] \qquad (6)$$

where $h_u = |\Delta u|$ and $h_v = |\Delta v|$ are the step sizes of the regular mesh of the reconstructed surface in the u and v directions respectively.

2.2. Modified VSF algorithm (MVSF)

In this work, a more accurate derivation process is proposed to get the discrete energy corresponding to the above continuous function (5). In particular, we propose to take into consideration higher element components of the corresponding two-variable Taylor formula. The discrete corresponding function is obtained by:

$$E_s(x) = \frac{h_u h_v}{2} \sum_{i,j} \left[\left(\frac{\mathbf{x}_{i+1,j} - 2\mathbf{x}_{i,j} + \mathbf{x}_{i-1,j}}{h_u^2} \right)^2 + \left(\frac{\mathbf{x}_{i,j+1} - 2\mathbf{x}_{i,j} + \mathbf{x}_{i,j-1}}{h_v^2} \right)^2 + \frac{1}{8} \left(\frac{\mathbf{x}_{i+1,j+1} - \mathbf{x}_{i+1,j-1} - \mathbf{x}_{i-1,j+1} + \mathbf{x}_{i-1,j-1}}{h_u h_v} \right)^2 \right] \quad (7)$$

We can see from the above expression that the first two terms are similar to the original formulation given in equation (6). They both use the so-called 5-star-points scheme. The main advantage of the expression given in equation (7) is its accuracy in using the 4 diagonal points to approximate the crossed second-order derivative at position (i,j), as shown in Figure 2a.

Obviously, Szeliski's approximation is a biased forward approximation, as shown in Figure 2b. The previous approximation is a biased approximation as presented in Figure 2a.

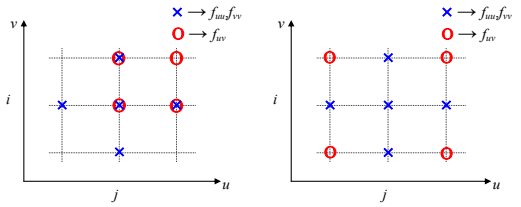

Figure 2 : Point estimation using VSF (a) and MVSF (b).

Reassembling all mesh points into a vector $\mathbf{X}$, we can rewrite equations (6) and (7) in a matrix form. The energy corresponding to the thin plate model can also be written in compact form as:

$$E(\mathbf{x}) = \frac{1}{2} \mathbf{x}^T \mathbf{A}_s \mathbf{x} \quad (8)$$

where the *stiffness* matrix $\mathbf{A}_s$ is a sparse matrix block diagonal matrix. The matrix $\mathbf{A}_s$ has at most 13 non-zero entries per row, as discussed in [7]. The rows with the maximum number of entries are : $(n + 1) \times M + (m + 2)$; $n = 1 : N - 4$ et $m = 1 : M - 4$; N et $M > 4$.

However, when periodicity is imposed upon the *stiffness* matrix $\mathbf{A}_s$, all rows would then have 13 non-zeros entries. Note that such periodicity constraint is appropriate when considering spherical coordinates used in describing human organs. The resulting *stiffness* matrix has a homogeneous structure and can be easily coded. It has been constructed following the method proposed by [8].

If $h_u = h_v = 1$, by imposing the continuity constraint, the stiffness matrix can be written in the following matrix form:

$$\mathbf{A}_s = \frac{1}{8} \begin{pmatrix} \mathbf{B} & \mathbf{C} & \mathbf{D} & \mathbf{0} & \cdots & \mathbf{0} & \mathbf{D} & \mathbf{C} \\ \mathbf{C} & \mathbf{B} & \mathbf{C} & \mathbf{D} & \mathbf{0} & \cdots & \mathbf{0} & \mathbf{D} \\ \mathbf{D} & \mathbf{C} & \mathbf{B} & \mathbf{C} & \mathbf{D} & \mathbf{0} & \cdots & \mathbf{0} \\ \mathbf{0} & \mathbf{D} & \mathbf{C} & \mathbf{B} & \mathbf{C} & \mathbf{D} & \mathbf{0} & \cdots \\ \vdots & \vdots & \vdots & \vdots & \vdots & \vdots & \vdots & \vdots \\ \mathbf{0} & \cdots & \mathbf{0} & \mathbf{D} & \mathbf{C} & \mathbf{B} & \mathbf{C} & \mathbf{D} \\ \mathbf{D} & \mathbf{0} & \cdots & \mathbf{0} & \mathbf{D} & \mathbf{C} & \mathbf{B} & \mathbf{C} \\ \mathbf{C} & \mathbf{D} & \mathbf{0} & \cdots & \mathbf{0} & \mathbf{D} & \mathbf{C} & \mathbf{B} \end{pmatrix} \quad (9)$$

where $\mathbf{B}$, $\mathbf{C}$ and $\mathbf{D}$ are $M \times N$ symmetric matrices. $\mathbf{0}$ is an $M \times N$ zero matrix.

2.3. Discrete problem

Using equations (4), (6) and (7), the combined discrete energy expression can hence be written in matrix form as:

$$E(\mathbf{x}) = \frac{1}{2} \mathbf{x}^T \mathbf{A}\, \mathbf{x} - \mathbf{x}^T \mathbf{b} + c \quad (10)$$

where $\mathbf{A} = \lambda \cdot \mathbf{A}_s + \mathbf{A}_d$, $\mathbf{b} = \mathbf{A}_d \cdot \mathbf{d}$ and c is a constant that may be omitted in the minimization process. This energy function has a minimum at $\mathbf{x} = \mathbf{x}^*$, which is the solution of the following linear system that is obtained via the Euler equation:

$$\mathbf{A}\, \mathbf{x}^* = \mathbf{b} \quad (11)$$

since $\mathbf{A}$ is a strictly positive matrix. The above set of linear equations is, hence, a high dimension homogeneous positive definite system, that can be solved using the conjugate gradient method, thanks to the strict positivity of the matrix $\mathbf{A}$. Our approximation is found to lead to better performance compared to that used in original VSF algorithm.

3. Data description

In this work, data consist of two sequences of surfaces of the left ventricle (LV) of the heart reconstructed within a cardiac cycle. Examinations were carried out on the same patient using successively two medical imaging modalities within a short period of time, in order to assume that the LV deformations are reproducible and hence medical comparisons would be applicable. The first sequence is composed of eight

LV surfaces obtained after automatic segmentation from nuclear medicine imaging (NMI), known to be a "gold standard" examination for cardiac observation.

The second LV sequence is provided by a multidimensional ultrasound technique (US) called LV4D for Left Ventricle in 4 Dimensions [4] [9], previously proposed by the authors. The objective was to use the NMI examination to validate this ultrasound method. The closed incomplete LV surfaces are first developed to a rectangular domain of size (I,J), with I = $[-\pi/2, +\pi/2]$ and J = $[0, 2\pi]$. The transformation between the two domains, spherical $S(x,y,z)$ (Figure 3a) and rectangular $D(\theta, \varphi)$ (Figure 3b), is obtained by using the following relations:

$x = \cos(\theta)\cos(\varphi)$, $y = \cos(\theta)\sin(\varphi)$, $z = \sin(\varphi)$.

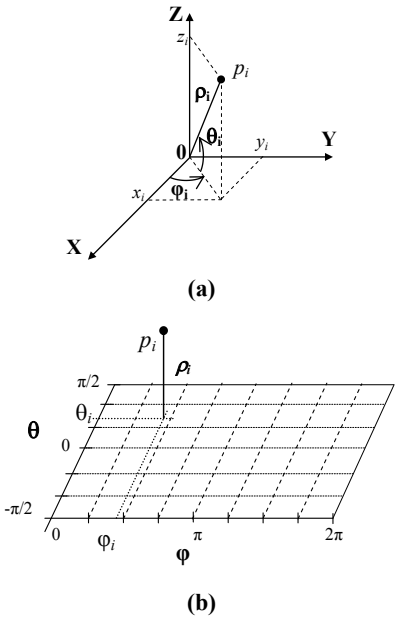

Figure 3 : Transformation of a point from spherical domain (a) to rectangular domain (b).

The associated surface of the spherical representation is identical to that of the rectangular surface. The samples of the developed surface are duplicated in (θ,φ) and placed in a doubly periodic grid according to these two variables. When the number of samples is too high (or the sampling grid is of reduced size), several samples $\{\rho i(\theta i,\varphi i)\}$ may correspond to the same element (i,j) in the grid. In this case, the average of these samples is taken at this position. By the same way, to reduce artefacts in $\theta=\pm\pi/2$, the average of samples available for each of these values of θ is assigned to all values of corresponding φ. In fact, the radius at the vertices of the closed surface are the same whatever the values of φ. In contrast, a sampling grid of large size, or a poor distribution of the initial samples of the reconstructed surface generates an incomplete grid.

Each missing value is then set to zero and its position is saved.

4. Results and discussion

4.1. Performance analysis

The results displayed in Figure 4 show that the proposed algorithm, MVSF, outperforms the original VSF algorithm, e.g. when the tolerance value of the iterative conjugate gradient algorithm is set to 10-4, the modified algorithm converges about 100 iterations faster than the original algorithm. One can also notice from Figure 4 that an inappropriate choice of the values of λ and w can induce a higher number of iterations to get the same value of MSE between the reference surface and the reconstructed one.

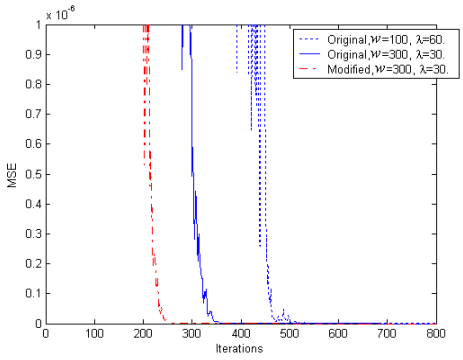

Figure 4 : Number of iterations necessary for the convergence of the two algorithms. Rate of convergence of the conjugate gradient algorithm.

Author names and affiliations are - or three-column format, with their affiliations italicized and centered below their respective names. Include e-mail addresses if possible. Author information should to be centered beneath the title and printed in Times 12-point, non-boldface type. Multiple authors may be shown in a two be followed by two 12-point blank lines.

4.2. Comparison of LV surfaces

In order for the given LV surfaces to be locally compared, the irregularity of the data, the number of the available data, or even the absence of certain samples requires the use of an interpolation step. The resampling of data was implemented to visualize the local differences of the compared surfaces. It was produced by the MVSF algorithm, Figure 5c, after

transformation of the Cartesian coordinates of the samples of original surfaces into spherical coordinates, Figure 5b.

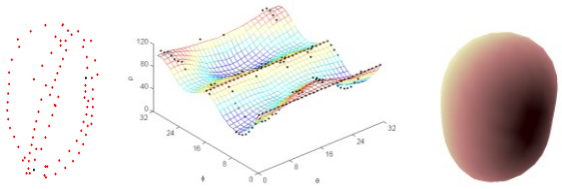

(a) (b) (c)

Figure 5 : Samples of a closed surface of a LV of heart (a). Reconstruction of surfaces by MVSF algorithm (b). Corresponding closed surface (c).

4.3. Global comparison

The evolution of the NMI and US LV volumes as a function of time provides a global comparison of the reconstructed surfaces, as shown on Figure 6. To facilitate the comparisons, each volume is normalized relative to a maximum volume obtained in diastole. From these volumes, measurements are realised: estimation of the telediastolic (V_D) and telesystolic (V_S) moments and volumes, then evaluation of the ejection fraction:

$$FE = \frac{V_D - V_S}{V_D} \qquad (12)$$

However, the lack of registration does not allow local comparisons, since the two surface absolute orientations are not known. The registration of the two sequences was performed by estimating the parameters of translation and rotation for each pair of corresponding surfaces of the two data sets using the CICP algorithm [10]. The sequence of surfaces obtained by scintigraphy served as a « reference », while the sequence of surfaces generated by ultrasound constructed the « target » data.

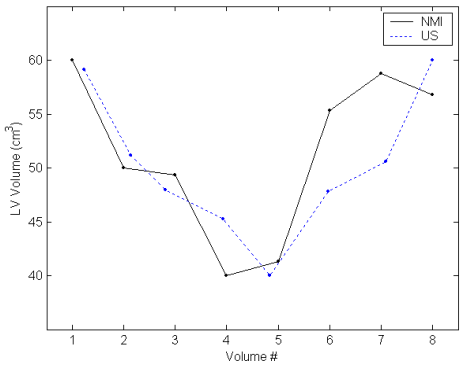

Figure 6 : Evolution of the NMI and US LV volumes.

It can be seen from this figure that the variation of evolution curves is comparable, even if a volume difference during diastolic phase is perceptible. This slight difference is probably explained by the unequal precise information obtained during surface estimation. In fact, the acquisition and reconstruction modes are very different for both techniques. However, the determination of the fraction of ejection, current measurement performed during the cardiac examination, gives results of the same order of magnitude, and sufficient precision to make a diagnosis, according to cardiologists:

$$F_{ej}\,(US) = 0{,}624 \approx F_{ej}\,(MN) = 0{,}706.$$

In this case, the reported fractions of ejection indicate normal cardiac contractions ($0{,}5 \leq F_{ej} \leq 0{,}7$).

4.4. Local comparison

Figure 7c presents an NM reconstructed surface of the left ventricle of heart using the proposed MVSF algorithm. A color coding allows cartograhing the distances between the surfaces obtained by the two modalities by visually local differences between the two registered surfaces.

From the medical point of view, the results presented in this study show that the surface provided by the LV4D method are close to the reference gated SPECT surface. Actually, for all considered surfaces, the coding of colors remains in average around the homogeneous light blue – green – yellow colors, indicating low radial distance between the two LV surfaces. These results validate the ultrasound LV4D method as an alternative to the reference gated SPECT examination.

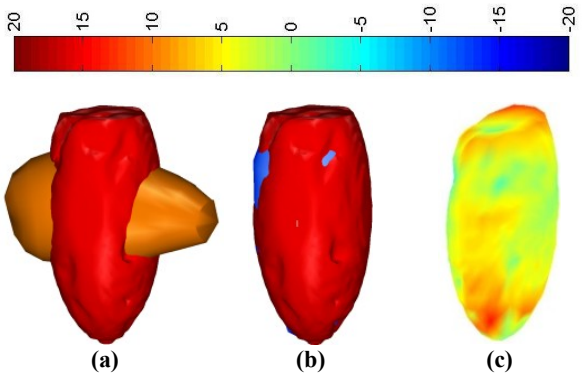

Figure 7 : Local comparison of two LV registered surfaces (c), acquired from gated SPECT (in red color) and ultrasound (in brown color before registration (a) and in blue color after registration (b)).

5. Conclusions and perspectives

The MVSF algorithm can be used to reconstruct closed surfaces of an organ of the human body, such as the left ventricle of the heart. It gives more precise surface reconstructions and is faster compared to its original VSF algorithm. However, the major drawback of both methods is the size of the rigidity matrices which increases in proportional to the square of the desired mesh. In fact, moving from a mesh of samples of 32×32 to a mesh of 64×64 results in moving from a dimension of stiffness matrix of 1024×1024 ($\sim 10^{+6}$) elements to 4096×4096 ($\sim 16\times 10^{+6}$). The size of the handled matrices, for a relatively small number of samples (4096) compared to the possibilities offered today by the medical imaging equipment, is an obstacle to the use of these variational splines based methods.

There exist already multi-scale methods to address this problem. Concerning the structure matrix presented in this work, it seems interesting to investigate whether a direct method, which would not require intermediate excessive storage, could not be developed to solve the linear system of equation (11).

Another research perspective could be to develop a 3D version of the MVSF algorithm in order to eliminate the step of converting Cartesian coordinates into spherical coordinates to convert closed surfaces into developed surfaces. Finally, it would be interesting to implement automatic methods to estimate the parameters of considered algorithms.

Using a reliable extension of the classical splines smoothing SVF method, the work presented in this paper describes a comparison technique based on color representation of the radial distances between two corresponding surfaces, projected on the surface of reference. It has been successfully applied to highlight differences between corresponding LV surfaces obtained starting from ultrasound and gated SPECT examinations. Finally, it was shown that the original LV4D method provides reconstructions of the LV surfaces equivalent to the surfaces obtained from gated SPECT, "gold standard" examination in the field of dynamic cardiac reconstruction. This result has a great medical interest, since the new method could be used as a promising alternative to the gated SPECT examination, taking all the benefits of the ultrasound modality: non invasive method, no radioisotope exposition, no contraindication, cost less expensive, mobile system.

The study presented can be extended to measure the differences between closed or developed corresponding surfaces (images). Then, it can be used to compare different reconstructions of a unique surface, or to compare a unique reconstruction of different surfaces. Additional work must be carried out to confirm the preliminary promising results. Particularly, focus should be done to improve the accuracy of samples that characterize the observed surfaces

6. References

[1] O. Garcia and A. Susin, “Left ventricle’s surface reconstruction and volume estimation”, Terceres jornades de recerca en Enginyeria Biomèdica, Spain, 2002.

[2] H. Hoppe, T. DeRose, T. Duchamp, J. McDonald, and W. Stuetzle, “Surface reconstruction from unorganized points”, the 19th annual conference on Computer graphics and interactive techniques, 1992.

[3] S. Gao and H.-Q. Lu, “A Fast Algorithm for Delaunay based Surface Reconstruction”, the 11th International Conference in Central Europe on Computer Graphics, Visualization and Computer Vision, China, 2003.

[4] C. Bonciu, R. Weber, and C. Léger, “4D reconstruction of the left ventricle during a single heart beat from ultrasound imaging”, *Image Vision Computing,*, 2001, vol. 19, pp. 401-412.

[5] Y. Wang and J. Wang, “Surface reconstruction using deformable models with interior and boundary constraints”, *IEEE Transaction. on Pattern Analysis & Machine Intelligence*, 1992, vol. 14, pp. 572-579.

[6] R. Enciso, J. P. Lewis, U. Neumann, and J. Mah, “3D Tooth Shape from Radiographs using Thin-Plate Splines”, the 11th Annual Medicine Meets Virtual Reality Conference, Newport Beach, California, 2003.

[7] R. Szeliski, “Fast surface interpolation using hierarchical basis functions”, *IEEE Transactions on Pattern Analysis & Machine Intelligence*, 1990, vol. 12, pp. 513-528.

[8] L. Sainsaulieu, *Calcul Scientifique*: Masson, 1996.

[9] C. Léger, “Contribution à l’échocardiographie multidimensionnelle”, *Habilitation à Diriger des Recherches, Université d’Orléans*, 2004.

[10] A. Almhdie, C. Léger, M. Deriche, and R. Lédée, “3D Registration Using a New Implementation of the ICP Algorithm Based on A Comprehensive Lookup Matrix: Application to Medical Imaging”, *Pattern Recognition Letters*, 2007, vol. 28, pp. 1383-1592.